Applied Catalysis B: Environmental 125 (2012) 538–545

Contents lists available at SciVerse ScienceDirect

Applied Catalysis B: Environmental

journal homepage: www.elsevier.com/locate/apcatb

In situ capture of active species and oxidation mechanism of RhB and MB dyes over sunlight-driven Ag/Ag_3PO_4 plasmonic nanocatalyst

Wei Teng[a], Xinyong Li[a,b,*], Qidong Zhao[a], Jijun Zhao[a], Dongke Zhang[b,**]

[a] Key Laboratory of Industrial Ecology and Environmental Engineering, School of Environmental Sciences and Technology & College of Advanced Science and Technology, Dalian University of Technology, Dalian, 116024, China
[b] Centre for Energy (M473), The University of Western Australia, 35 Stirling Highway, Crawley WA 6009, Australia

ARTICLE INFO

Article history:
Received 12 March 2012
Received in revised form 18 May 2012
Accepted 27 May 2012
Available online 5 June 2012

Keywords:
Photocatalysis
Sunlight
Ag/Ag_3PO_4
Calculation

ABSTRACT

Sunlight-driven Ag/Ag_3PO_4 plasmonic nanocatalysts have been successfully prepared using an in situ ethylene glycol reduction method. The photocatalysts showed strong photocatalytic activity for decomposition of RhB and MB dyes under visible light irradiation ($\lambda > 420$ nm). The excellent photocatalytic performance of Ag/Ag_3PO_4 came from the sensitivity of Ag_3PO_4 and the high separation efficiency of electron–hole pairs, which resulted in a large number of holes participating in the photocatalytic oxidation process. The results of density function theory calculation revealed that the visible-light absorption band in the Ag_3PO_4 catalyst is attributed to the band transition from the hybrid orbital of O 2p and Ag 4d to the Ag 5 s and 5p orbital. The generation of active species in the photocatalytic system was evaluated using the fluorescence (FL) and electron spin resonance (ESR) techniques as well as in situ capture of active species by t-butanol and EDTA. The results indicated that the free hydroxyl radicals were not the major active oxidizing species in the photocatalytic process. The photocatalytic reaction process of the pollutants was mainly governed by the direct oxidation by the holes.

1. Introduction

Dyes are commonly used in many industries to color their finished parts and products. During dyeing processes, more than 15% of the dyestuff does not bind to the fibers or surfaces and is therefore released into the wastewater stream [1]. Many dyes and their reaction products are very harmful to the environment and human and animal health due to the presence of toxic or even carcinogenic [2–5]. Semiconductor photocatalysis has been extensively studied and applied as a viable control method for such pollution [6–10]. Recent research has shown that TiO_2-based heterogeneous photocatalytic oxidation is still the most promising water treatment method [11–16]. Nevertheless, the poor solar efficiency has hindered the commercialization of this technology. Thus, it is of great interest to develop photocatalysts that can yield high reactivity under visible light in order to overcome the drawbacks of TiO_2 [17–21]. Silver-based oxides are found to be promising alternatives and have been widely employed in research into the photocatalytic reactions [22–24]. However, the results reported so far are still far from ideal. Recently, Yi et al. reported a new use for the Ag_3PO_4 semiconductor, which can harness visible light to oxidize and degrade water borne organic contaminants in aqueous solutions [25]. Bi et al. developed a facile and general route for high-yield fabrication of single-crystalline Ag_3PO_4 rhombic dodecahedrons with only facets exposed and cubes bounded entirely by the {1 0 0} facets [26]. Their studies indicated that rhombic dodecahedrons exhibit much higher activities than cubes for the degradation of aqueous organic contaminant. However, the electrons generated in the photocatalytic process combine with mobile interstitial silver ions, leading to the decomposition of the catalyst [27]. This indicates that Ag_3PO_4 is unstable under the irradiation of light. The Ag^0 species on the surface of the catalyst probably enhances the electron–hole separation and the interfacial charge transfer. Liu et al. has prepared Ag/Ag_3PO_4 photocatalyst by one-pot hydrothermal method assisted by pyridine [28]. Furthermore, the main oxidative species (h^+ or $^\bullet OH$) in the photocatalytic degradation are still unclear and the photocatalytic mechanism of the oxidation of dyes over Ag/Ag_3PO_4 is yet to be understood.

In the present contribution, we report a new type of photocatalysts using a Ag/Ag_3PO_4 composite synthesized using the in situ ethylene glycol reduction method. MB and RhB were chosen as model pollutants to evaluate the photocatalytic activity in aqueous medium under visible light irradiation. The results obtained indicated that the Ag/Ag_3PO_4 composite can photocatalytically degrade

* Corresponding author. Key Laboratory of Industrial Ecology and Environmental Engineering, School of Environmental Sciences and Technology & College of Advanced Science and Technology, Dalian University of Technology, Dalian, 116024, China. Tel.: +86 411 8470 7733; fax: +86 411 8470 8084.
** Corresponding author. Tel.: +61 8 6488 7600; fax: +61 8 6488 7235.
E-mail addresses: xyli@dlut.edu.cn (X. Li), dongke.zhang@uwa.edu.au (D. Zhang).

0926-3373/$ – see front matter © 2012 Elsevier B.V. All rights reserved.
http://dx.doi.org/10.1016/j.apcatb.2012.05.043

RhB and MB under visible light irradiation with excellent efficiency. The further theoretical calculation based on density functional theory (DFT) helped to clarify the relation between photocatalytic activity and electronic structure. The possible photodegradation mechanism was studied by examining the active species OH, O_2^- anions, or h^+ through adding their scavengers such as t-Butanol and EDTA. In addition, the ESR and FL techniques with terephthalic acid (TA) technique were also used to monitor the active species formed in the photocatalytic process [29].

2. Experimental

2.1. Sample preparation

All chemicals used were analytical grade reagents without further purification. The Ag/Ag_3PO_4 plasmonic nanocatalysts were prepared according to the methods which developed recently [30]. 0.7 mmol $NaH_2PO_4{\cdot}2H_2O$ and 54 mg poly (vinyl pyrrolidone) (PVP) were sequentially added to 12 ml of ethylene glycol in a 20 ml vial to form solution 1 and was heated to 60 °C. 1 mmol $AgNO_3$ was added to 3 ml ethylene glycol at room temperature to form solution 2 and was injected via a pipette to solution 1 above. The mixed solution was stirred at 60 °C for 30 min, resulting in the formation of a cream dispersion containing Ag_3PO_4 nanoparticles (RT_0). The vial containing the cream dispersion was then transferred to an oil bath set at 160 °C and continuously stirred for reduction over different periods of time. The reduction time (RT) was set 20 min, 40 min, 60 min, and 80 min to produce a series of photocatalysts denoted as RT_{20}, RT_{40}, RT_{60}, and RT_{80}, respectively. At the end of each reduction period, the vial was taken out of the oil bath and cooled in the air to room temperature. The solids were filtered and then washed several times with distilled water and ethanol. Finally the as-prepared samples were dried in air at 70 °C over night. A schematic diagram of the catalyst preparation process is shown in Fig. S1.

2.2. Characterization

X-ray diffraction (XRD) analysis of the photocatalysts was performed using a Rigaku D/max- γb diffract meter with Cu Kα radiation, operating at 40 kV and 200 mA (λ = 0.1542 nm). The morphology of the samples was observed using a field-emission scanning electronmicroscope (FE-SEM, Hitachi S-4800, Tokyo, Japan) with an accelerating voltage of 3.0 kV, equipped with an energy-dispersive X-ray analysis (EDX) system. UV–vis diffusive reflectance spectrums (DRS) of the samples were measured by using a Shimadzu UV-2450 UV-vis spectrophotometer.

2.3. Theoretical calculation

The calculations were performed using a first-principle pseudopotential method based on the density-functional theory (DFT), as implemented in the Cambridge serial total energy package (CASTEP) code [31]. The structure was optimized. The GGA in the PBE0 functional formalism was applied combined with norm-conserving pseudopotentials [32]. The *k*-point meshes for Brillouin zone sampling were constructed using the Monkhorst–Pack scheme. A plane wave cutoff energy of 550 eV was used.

2.4. Photocatalytic activity test

The photocatalytic activity of the Ag/Ag_3PO_4 plasmonic nanocatalysts was evaluated by studying the degradation of RhB and MB under visible light irradiation. The light source used was a 500 W high pressure xenon lamp (Shanghai Lanpu Light, China) with a 420 nm cut-off filter. The intensity of the light, as measured using a Vis-irradiance meter (FZ-A, Instrument Factory, Beijing Normal University), was 11.3 mW cm^{-2}. The photocatalytic degradation of RhB and MB was carried out at room temperature in a quartz photochemical reactor containing 50 mg catalyst and RhB or MB aqueous solution (50 ml, 20 mg L^{-1}). Before illumination, the suspension was stirred for 30 min in dark to ensure the establishment of an adsorption and desorption equilibrium. 3 ml liquor were collected at certain time intervals and centrifuged to remove the solid catalyst particles. The filtrates were analyzed by recording variations of maximum absorption band (552 nm for RhB and 660 nm for MB) using a UV-vis spectrophotometer (JASCO V-550). A total organic carbon (TOC) analyzer (Shimadzu TOC-5000) was employed to determine the mineralization of the RhB and MB solutions. The photocatalytic activity of the Ag/Ag_3PO_4 plasmonic nanocatalyst was also evaluated by decomposing RhB and MB under natural sunlight in Dalian city (13:00 p.m. to 13:20 p.m.; October 20th, 2010). The method was similar to the tests under the visible light in laboratory as described above. The active species generated in the photocatalytic system were detected with an in situ capture technique using the t-BuOH and EDTA tests. The generation of •OH radicals was investigated using the ESR (Bruker spectrometer E 500) and FL (Hitachi F-4500, Tokyo, Japan) technique.

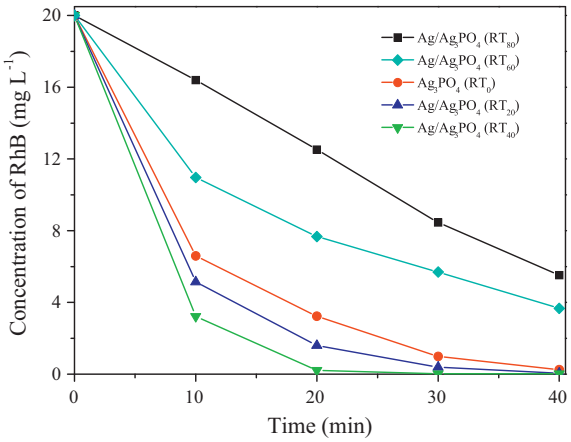

Fig. 1. Photocatalytic degradation of RhB over the as-prepared samples under visible light irradiation (λ > 410 nm).

3. Results and discussion

3.1. Photocatalytic performance

Fig. 1 shows the degradation of RhB in the aqueous solution as a function of exposure time in the presence of the Ag/Ag_3PO_4 plasmonic nanocatalysts with varying reduction time (RT_0, RT_{20}, RT_{40}, RT_{60} and RT_{80}) under visible light irradiation. When the RT was below 40 min, the photocatalytic activity of the photocatalyst increased with the RT increase of RT. The complete photodegradation of RhB used 40, 30 and 20 min for RT_0, RT_{20} and RT_{40} catalyst, respectively. However, when RT was further increased to 60 and 80 min (RT_{60}, RT_{80}), the photocatalytic activity of the photocatalyst decreased gradually. The degradation rate of RhB was 81.65% and 72.4% for RT_{60} and RT_{80} after 40 min irradiation. Furthermore, the rate of the photodegradation process was fitted using a pseudo-first-order kinetic model (Fig. S2). The apparent reaction rate constant *k* was found to be 3.0×10^{-2}, 4.4×10^{-2}, 1.0×10^{-1}, 1.4×10^{-1} and 2.2×10^{-1}, respectively, for the RT_{80}, RT_{60}, RT_0, RT_{20} and RT_{40} plasmonic nanocatalyst. These observations suggest that the reduction time had a significant influence on the photocatalytic activity of the photocatalysts and the as-prepared photocatalyst RT_{40} had the highest photocatalytic activity, with 100% of RhB decomposed within 20 min.

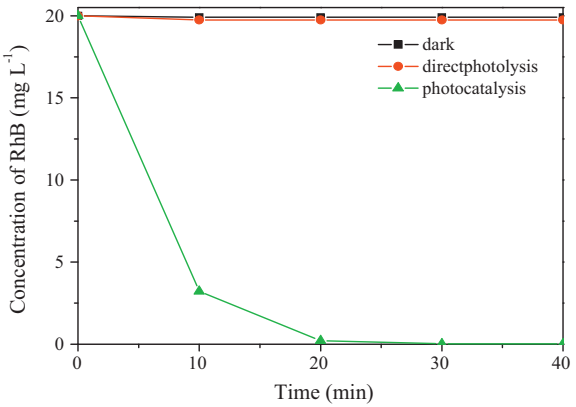

Fig. 2. Degradation of RhB by Ag/Ag_3PO_4 (RT_{40}) under different conditions. Inset: absorption changes of RhB solution under photocatalytic process. Inset: Degradation of 2-CP by Ag/Ag_3PO_4 (RT_{40}) with different process.

It can be explained that moderate of Ag nanoparticles on the surface of Ag_3PO_4 can facilitate the transformation of the photoinduced electrons and reduce the combination of electron–hole pairs. This includes both the size and amount of Ag nanoparticles. However, with further increasing RT, too much and big Ag particles would accumulate on the surface of Ag_3PO_4, which adversely affects the light absorption of the Ag_3PO_4 photocatalyst, resulting in a decrease in the photocatalytic efficiency. For comparison, RhB adsorption on these photocatalyst in dark and the RhB photodegradation under visible light were performed. The results are presented in Fig. 2. The test confirmed that RhB did not degrade in the dark nor in the absence of photocatalysts under visible light irradiation. These observations confirm that the adsorption action of photocatalysts and photolysis were not responsible for the disappearance of RhB in the photodegradation experiments and the photocatalytic effect of Ag/Ag_3PO_4 can be ascertained. In addition, to further evaluate and compare the photocatalytic performance of the Ag/Ag_3PO_4 nanocatalyst in the elimination of aqueous contaminants, the decomposition of 2-Chlorophenol (2-CP) was also studied (inset of Fig. 2). These results confirm that the as prepared Ag/Ag_3PO_4 plasmonic nanocatalyst have the efficient visible light photocatalytic activity both on dyes and other organic pollutants.

The temporal evolution of the spectral changes taking place at 554 nm during the photodegradation of RhB over Ag/Ag_3PO_4 is shown in Fig. 3a. The photocatalytic activity of Ag/Ag_3PO_4 was also estimated by monitoring the successive decrease in the absorption intensity of MB at 662 nm as shown in Fig. 3b. The color of the suspension changed sequentially from pink and blue to colorless respectively as shown in the inset of Fig. 3a and b. The mineralization behavior of RhB and MB over the plasmonic nanocatalysts was

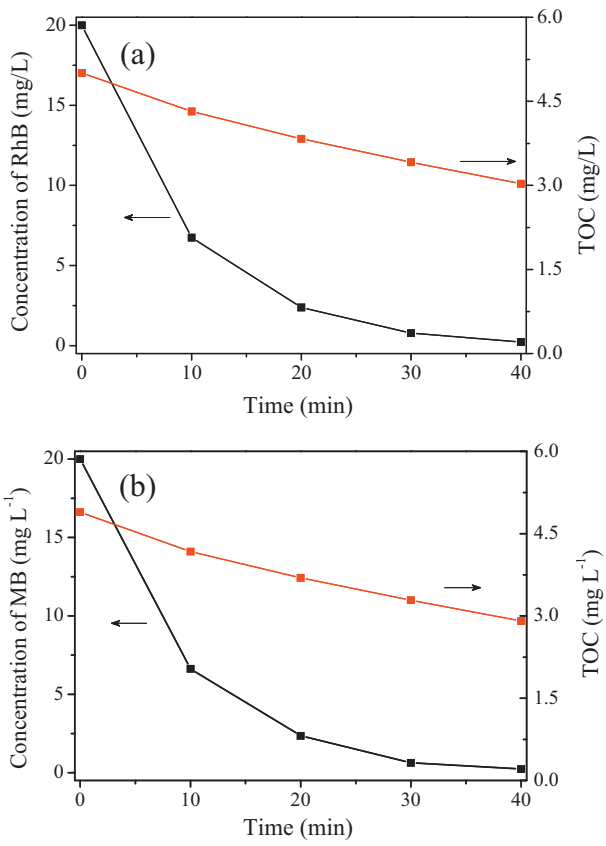

Fig. 4. Temporal change in Dye and TOC removal in the presence of Ag/Ag_3PO_4 (RT_{40}): (a) for RhB and (b) for MB. The initial RhB/MB concentration was 20 mg L^{-1}, the catalyst amount was 1.0 g L^{-1}.

also examined. The results are shown in Fig. 4. The mineralization rates of RhB and MB after 40 min photodegradation were found to be 39.5% and 40.6%, respectively. However, the photodegradation rates of RhB and MB were achieve 100% after 40 min photocatalysis. The results indicate that the mineralization rate was slower than that of discoloration of dyes. In other words, the chromophore of the dye molecules were destroyed, but not completely mineralized to inorganic molecules.

To further investigate the activity of the plasmonic nanocatalysts, the degradation of RhB and MB under the real sunlight irradiation conditions was determined and the results are shown in Fig. 5. It can be revealed that the plasmonic nanocatalysts as prepared exhibited excellent photocatalytic activity in real sunlight for the photodegradation of MB and RhB with nearly 100% degradation achieved in merely 10 min.

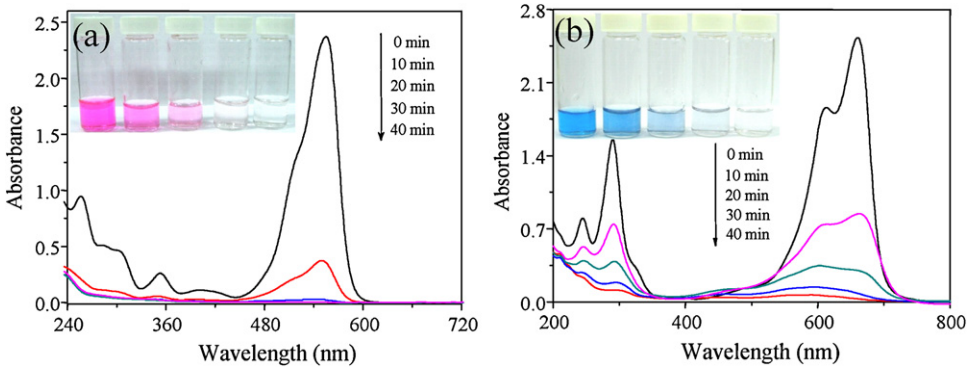

Fig. 3. Absorption changes of (a) for RhB and (b) for MB solution under photocatalytic process.

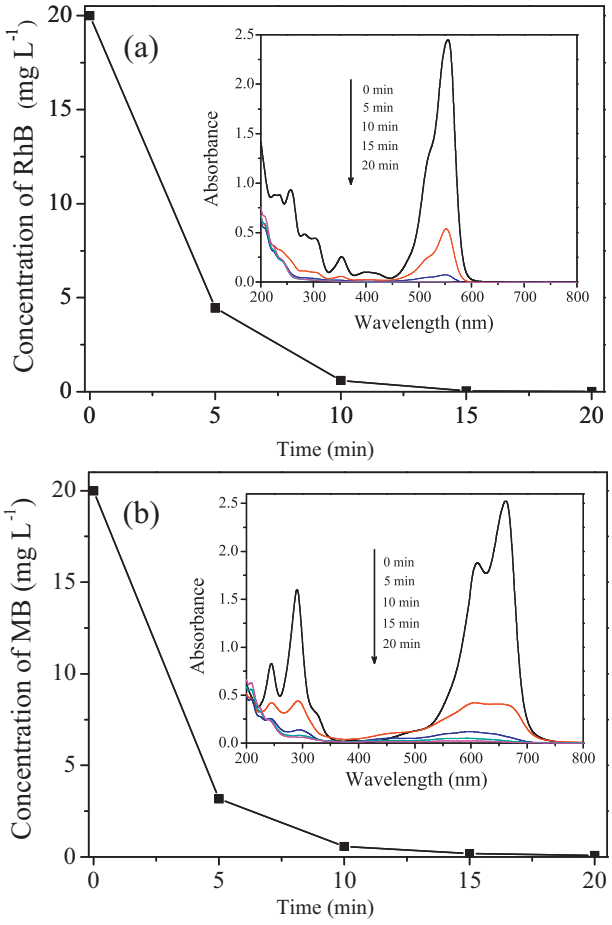

Fig. 5. Plots of photodegradation of (a) RhB and (b) MB by Ag/Ag_3PO_4 (RT_{40}) under natural sunlight irradiation conditions.

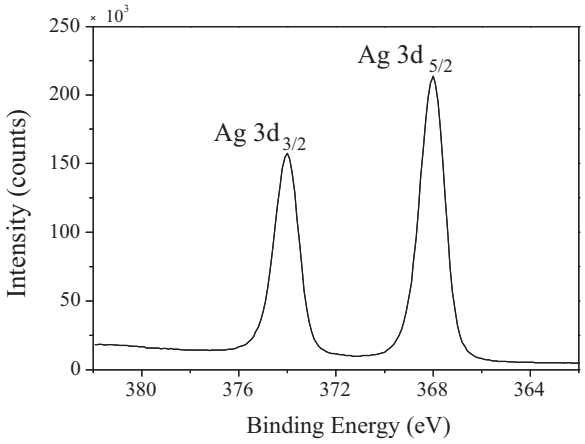

Fig. 7. Typical XPS spectra of Ag 3d of Ag/Ag_3PO_4 plasmonic nanocatalyst.

3.2. Structure and optical properties of Ag/Ag_3PO_4

Fig. 6 shows typical SEM images and spot EDX data of the Ag_3PO_4 plasmonic nanocatalysts, (a) Ag_3PO_4; (b) Ag/Ag_3PO_4 (RT_{40}); (c) Ag/Ag_3PO_4 (RT_{80}) and (d) EDX of Ag/Ag_3PO_4 (RT_{40}). Fig. 6a suggests that the average size of the Ag nanoparticles on Ag_3PO_4 was estimated to be 0.5–1 μm and the surface was relatively smooth. Fig. 6b and c shows the SEM images of Ag nanoparticles deposited on Ag_3PO_4 with the RT_{40} and RT_{80}, respectively. It is clearly evident from Fig. 6b that a small number of the Ag nanoparticles were present on the surface of Ag_3PO_4. The size of the Ag nanoparticles ranged from 10 to 20 nm, consistent with the XRD result. As the RT was extended, there were more Ag nanoparticles formed on the surface of Ag_3PO_4 particles, as shown in Fig. 6c, and the size of the Ag nanoparticles increased to 30–50 nm. Fig. 6d shows the EDX spectrum, further confirming that the as-prepared photocatalysts were composed of Ag, P and O.

Moreover, the X-ray photoelectron spectroscopy (XPS) of our Ag/Ag_3PO_4 plasmonic nanocatalyst was examined, as shown in

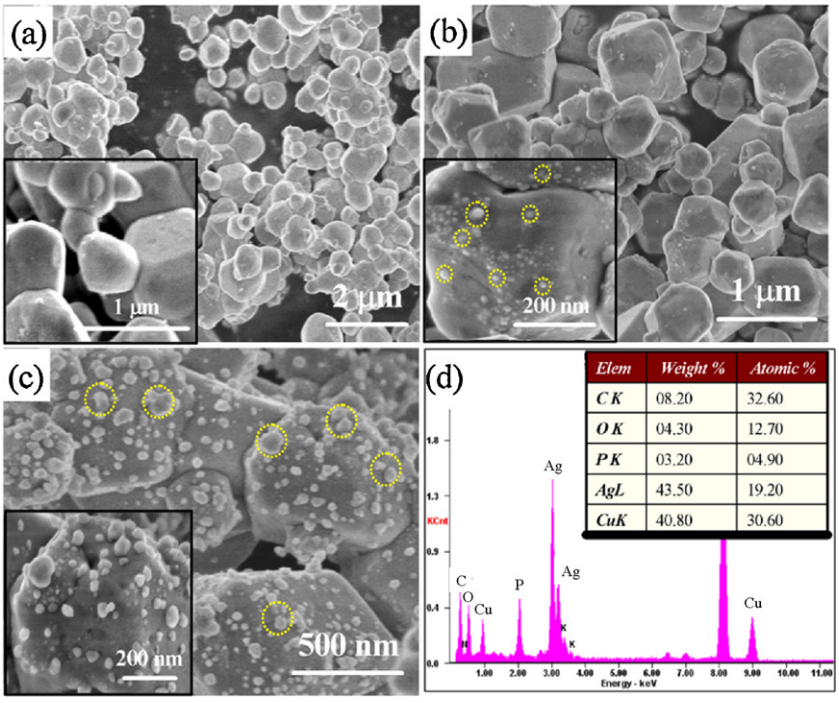

Elem	Weight %	Atomic %
C K	08.20	32.60
O K	04.30	12.70
P K	03.20	04.90
Ag L	43.50	19.20
Cu K	40.80	30.60

Fig. 6. SEM images of (a) Ag_3PO_4; (b) Ag/Ag_3PO_4 (RT_{40}); (c) Ag/Ag_3PO_4 (RT_{80}) and (d) EDX of Ag/Ag_3PO_4 (RT_{40}).

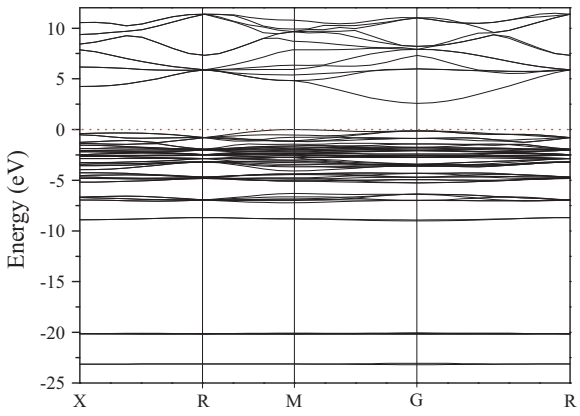

Fig. 8. Band structure of Ag_3PO_4. The position of Fermi level is set to be 0 eV.

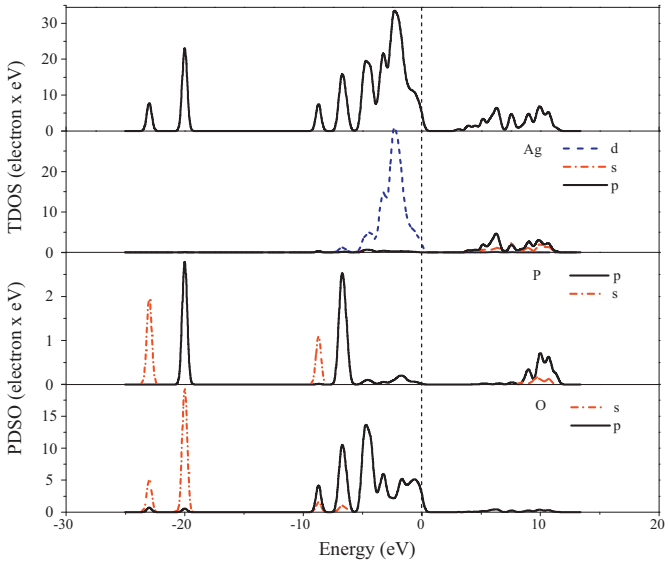

Fig. 9. PDOS and TDOS of Ag_3PO_4.

Figure S3. It was found that the peaks were a result of elements Ag, P and O. The detailed spectra for Ag are shown in Fig. 7. There are two bands at 367.8 and 373.8 eV, ascribed to Ag $3d_{5/2}$ and Ag $3d_{3/2}$ binding energies are observed, respectively. Where the band at 373.8 eV is attributed to the Ag^+ of Ag_3PO_4 and those at 367.8 is ascribed to the metallic Ag^0. Similar results are reported by other researchers [33,34]. The Ag $3d_{3/2}$ and Ag $3d_{5/2}$ peaks can be further divided into two different peaks at 374.0, 373.4 eV and 368.0, 367.5 eV, respectively. According to the results reported by Arabatzis et al. and Liu et al. [28,35], the peaks at 374.0 and 368.0 eV can be attributed to Ag^0, whereas the peaks at 373.4 and 367.5 eV are attributed to Ag^+ ions of Ag_3PO_4. These results verify the existence of metallic Ag^0 in our Ag/Ag_3PO_4 species, Figure S4 shows the XRD patterns of the Ag_3PO_4 and Ag/Ag_3PO_4 plasmonic nanocatalysts, respectively. The diffraction peaks of those catalysts can be indexed to Ag_3PO_4 [JCPDS No. 08-0505]. In addition, both of the peaks located at 38.11° and 44.28° belonged to Ag [JCPDS No. 04-0783]. However, because the amount of Ag is so small that it is beyond the detection of XRD, no distinct peaks corresponding to Ag were observed in the Ag/Ag_3PO_4 sample RT_{40}. The peaks corresponding to monoclinic Ag appeared in the RT_{80} catalyst (shown in Fig. S4 curve a).

The DRS of the Ag_3PO_4 and Ag/Ag_3PO_4 plasmonic nanocatalysts with different RT are depicted in Figure S5. The Ag_3PO_4 sample showed an absorption edge around 530 nm, which could be responsible for the visible light induced photocatalytic activity. With the loading of Ag, the Ag/Ag_3PO_4 displayed the same absorption edge as Ag_3PO_4. The absorption intensity increased when the RT increased from 20 min to 40 min, but decreased when the RT increased from 60 min to 80 min (shown in the inset of Figure S5). This suggests that an appropriate amount of the silver nanoparticles loaded on the surface of Ag_3PO_4 can benefit the absorption of light for the plasmonic nanocatalysts but excessive amounts of the Ag nanoparticles may retard the absorption of light for catalysts. On the basis of the equation: $\alpha h\nu = A\,(h\nu - E_g)^{n/2}$ [36,37], where α, ν, E_g, and A are the absorption coefficient, the light frequency, the band gap, and a constant, respectively. Among them, n depends on whether the transition is direct ($n = 1$) or indirect ($n = 4$). The value of n for Ag/Ag_3PO_4 plasmonic nanocatalyst was 1 from the data in Figure S5. The band gap of the photocatalyst was estimated to be 2.33 eV from the onset of the absorption edge from Figure S6.

3.3. Electronic properties calculation of Ag_3PO_4

The energy level and the band gap of the oxide semiconductor will play a crucial role in determining its photocatalytic activity, In the present study, the electronic structure of Ag_3PO_4 was investigated by hybrid-DFT approaches, The result is shown in Fig. 8. The Fermi level indicated by dashed line is set as zero. The calculation results revealed that Ag_3PO_4 is an indirect gap semiconductor from Fig. 8. The band structure of Ag_3PO_4 shows that the top of the valence band (VB) is located at M point. And the energy minimum of the lowest conduction band (CB) was located at G point. As shown in Fig. 8, the indirect band gap between M and G is 2.57 eV, which agrees roughly with the experimental value 2.33 eV.

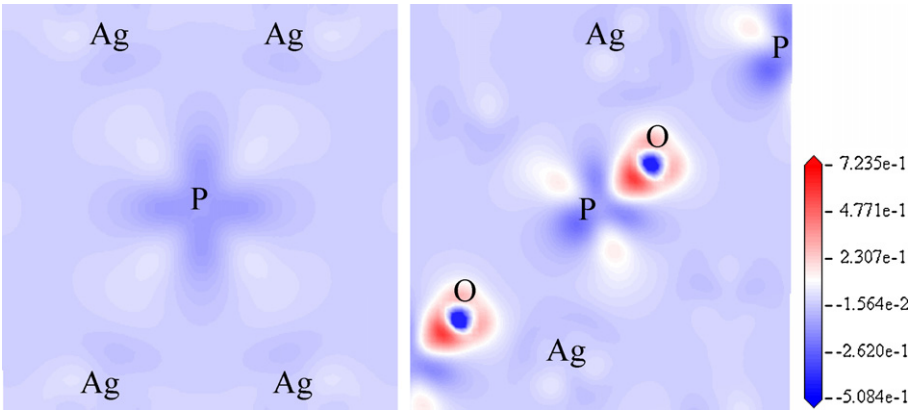

Fig. 10. Analysis of the charging density of Ag_3PO_4.

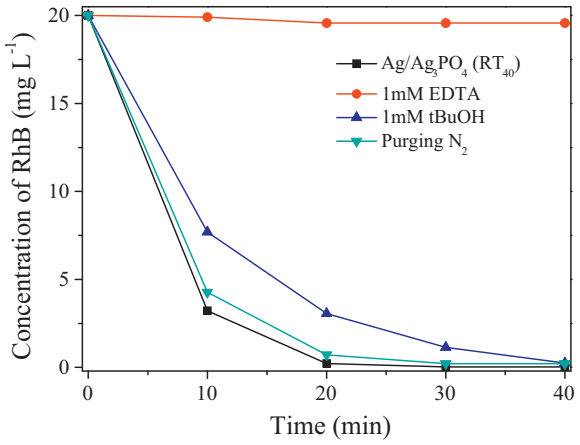

Fig. 11. Plots of photogenerated active species trapped in the system of photodegradation of RhB by Ag/Ag$_3$PO$_4$ (RT$_{40}$) under visible light irradiation.

The total and partial density of states (TDOS and PDOS) is shown in Fig. 9. The bottom of the conduction band mainly consist of 4s band of Ag. Above the Fermi level, the bottom of the conduction bands is dominated by Ag 5s and 5p orbital. Near the Fermi level, the top of the valence bands are derived from O 2p and Ag 4d states. Furthermore, it can be observed from the Fig. 9 that the dispersion of O 2p is wider than that of Ag 4d states. This will be beneficial to the transition of electrons from valence band to conduction band.

In order to further investigate the bonding behavior between the atoms, we have presented the electron density difference maps in the planes containing O, P and Ag ions, respectively. As shown in Fig. 10, the electron mainly accumulates around the O atom. Furthermore, it can be seen from the Fig. 10 that there is interaction of charges between O and P due to O 2p and P 3s hybridization, thus showing that there is covalent bonding between O and P. The charge distribution around the Ag is comparatively negligible and as a result the Ag atom is fairly isolated, which could indicate that the bonding between Ag and PO_4 is mainly governed by ionic.

3.4. Investigation of active species in photocatalytic degradation of RhB

The main active species in the photocatalytic process were examined in the experiments of in situ capture of active pieces. As shown in Fig. 11, the photodegradation of RhB was slightly inhibited by the addition of t-BuOH (hydroxyl radicals scavenger) under visible light irradiation, indicating that the free hydroxyl radicals were not the major active oxidizing species in the photocatalytic process. However, it was intensively suppressed when EDTA (holes scavenger) was introduced. This indicates that holes were the main active oxidizing species involved in the photoreaction process. The direct hole transfer mainly governs the photocatalytic process, which is consistent with the literature reports [38,39]. Meanwhile, O_2^- may also serve as active species in this reaction. N_2 was used to confirm the effect of O_2 and the results are shown in Fig. 11. Under the anoxic suspension, the degradation of RhB was not inhibited, indicating that O_2^- was not the main active species either. To further confirm these results, the system was examined using the FL spectroscopy to monitor the active radicals during the photocatalytic reaction process. It is well known [40] that •OH reacts with TA and generates 2-hydroxy terephthalic acid (TAOH), which emits fluorescence at around 426 nm on the excitation of its own 312 nm absorption band. As shown in Fig. 12a, the fluorescence intensity at 426 nm was not significantly changed with the irradiation time extended, indicating that •OH was not produced on the Ag/Ag$_3$PO$_4$ plasmonic nanocatalyst

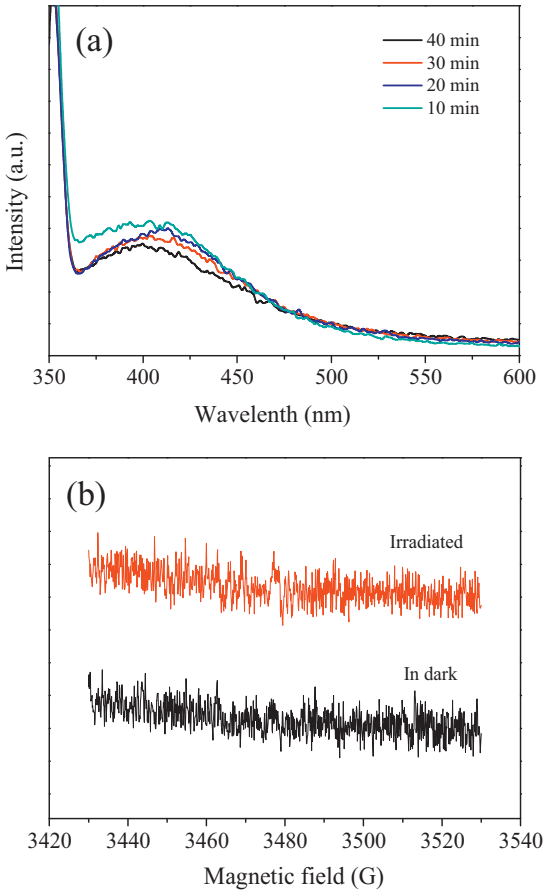

Fig. 12. (a) •OH trapping FL spectra of Ag/Ag$_3$PO$_4$ on TA solution under visible irradiation and (b) DMPO spin-trapping ESR spectra recorded at ambient temperature in Ag/Ag$_3$PO$_4$ suspension under VL irradiation (λ = 532 nm) for DMPO-•OH in aqueous dispersion.

under visible light irradiation. To further prove this hypothesis, the ESR spin-trap technique 5, 5-dimethyl-l-pyrroline N-oxide (DMPO) was employed to probe the nature of the reactive oxidizing species generated on the surface of the Ag/Ag$_3$PO$_4$ under visible-light irradiation. No signals were detected either when the RhB and suspension were placed in dark or under visible light in the ESR spectrum as shown in Fig. 12b. These results suggest that •OH and $•O_2^-$ were not the major active oxidizing species in the photocatalytic process under visible light irradiation. These leave us with the only plausible explanation that the degradation process of dyes was mainly governed by direct oxidation by the holes.

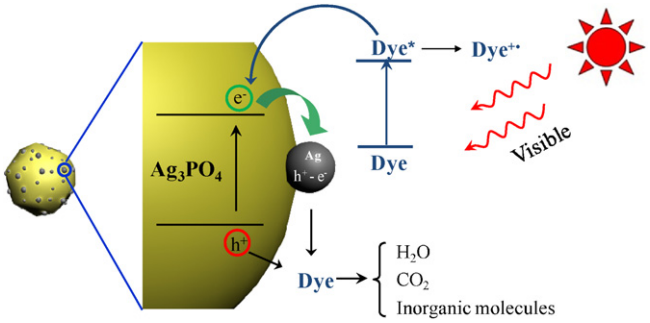

Scheme 1. The proposed photodegradation mechanism of the dye molecules on the surface of Ag/Ag$_3$PO$_4$ plasmonic nanocatalyst.

3.5. Photocatalytic mechanism

A possible mechanism is proposed to explain the high photocatalytic activity of the as-prepared Ag/Ag_3PO_4 plasmonic nanocatalyst, as shown in Scheme 1. The visible light can be absorbed efficiently by both the Ag_3PO_4 and the silver nanoparticles. Electrons in the valence band of Ag_3PO_4 could be excited to the conduction band and a large amount of electron–hole pairs are then generated. The electrons generated from Ag_3PO_4 can transfer quickly towards Ag nanoparticles, so that the Ag^+ of the Ag_3PO_4 nanocatalyst can escape from the reduction by these excess electrons to the maximum extent, which ensures the stability of the catalyst. The holes generated on Ag_3PO_4 could then oxidize the dyes molecule directly [41]. The degradation of dyes was mainly governed by the direct oxidation of the holes, which has been proved experimentally above. Part of the excess electrons in the conduction band of Ag_3PO_4 could transfer to the Ag nanoparticles, when they behave as the electron acceptor. However, some of the electrons accumulating in the conduction band of Ag_3PO_4 will lead to the reduction of Ag^+ of Ag_3PO_4, which may explain why the photocatalytic efficiency displays a slight decrease after the reaction is performed consecutively five times.

Considering the surface plasmon resonance (SPR) of the Ag nanoparticles, the photo-induced h^+ on silver nanoparticles can also oxidize the dye molecule directly [41–43]. In addition, the excellent conductivity of the silver nanoparticles enhances the interfacial charge transfer and stops the recombination of electron–hole pairs effectively. Then the excess electrons accumulating on the surface of Ag nanoparticles will go to reduce the dye molecules, or are trapped by O_2 and H_2O at the surface of photocatalyst in the solution to form O_2^- or $O_2^{-\bullet}$ reactive oxygen species [44,45]. These reactive oxygen species also help degrade the dye molecules.

Meanwhile, the dye molecules are excited by the absorption of visible light [46,47], and electrons are injected into the conduction band of Ag_3PO_4 or the silver nanoparticles, facilitating the oxidation of the dye molecules. Part of the excess electrons in the conduction band of Ag_3PO_4 will further transfer to the Ag nanoparticles, which behave as the electron acceptor. During the degradation of dye pollutants, some organic radicals or active oxidizing species could be also formed following the photo-induced electron injection from the dyes into Ag_3PO_4, which could attack other co-existing pollutants to provoke their decontamination under visible light irradiation. Finally, we stress that the transfer of the electrons from both the dyes and the conduction band of Ag_3PO_4 into the silver nanoparticles avoids the capture by Ag^+ of Ag_3PO_4, which ensures the stability of the composite catalyst.

4. Conclusions

In summary, we have synthesized sunlight-driven Ag/Ag_3PO_4 plasmonic nanocatalysts using the in situ ethylene glycol reduction method and their photocatalytic properties were tested in dyes oxidation. The new photocatalysts have exhibited strong photocatalytic activity under visible light irradiation. The theoretical calculation based on DFT indicates that the bottom of the conduction bands is dominated by Ag 5s and 5p orbital. And the top of the valence bands are derived from O 2p and Ag 4d states. The excellent photocatalytic performance of the Ag/Ag_3PO_4 has been attributed to not only the super sensitivity of Ag_3PO_4 to light, but also the high separation efficiency of electron–hole pairs on the surface of Ag_3PO_4. Moreover, the generation of active species in the photocatalytic system has been detected using the in situ capture of using t-Butanol and EDTA and analyzed using FL and ESR. The results have suggested that the mechanism of the dye oxidation over the sunlight-driven Ag/Ag_3PO_4 plasmonic nanocatalyst be the direct oxidation by the holes.

Acknowledgments

This work was supported financially by the National Nature Science Foundation of China (NSFC-RGC 21061160495), the National High Technology Research and Development Program of China (863 Program) (2010AA064902), the Excellent Talents Program of Liaoning Provincial University (LR2010090) and China's One Thousand Chinese Talents Award and the Australia Research Council under the Linkage Project Scheme (Project Numbers: LP0989368 and LP100200136).

Appendix A. Supplementary data

Supplementary data associated with this article can be found, in the online version, at http://dx.doi.org/10.1016/j.apcatb.2012.05.043.

References

[1] H. Park, W. Choi, Journal of Photochemistry and Photobiology A 159 (2003) 241–247.
[2] I.K. Konstantinou, T.A. Albanis, Applied Catalysis B 49 (2004) 1–14.
[3] A. Kar, Y.R. Smith, V.R. Subramanian, Environmental Science and Technology 43 (2009) 3260–3265.
[4] F.J. Cervantes, A. Garcia-Espinosa, M.A. Moreno-Reynosa, J.R. Rangel-Mendez, Environmental Science and Technology 44 (2010) 1747–1753.
[5] C.E. Clarke, F. Kielar, H.M. Talbot, K.L. Johnson, Environmental Science and Technology 44 (2010) 1116–1122.
[6] M.M. Haque, M. Muneer, D.W. Bahnemann, Environmental Science and Technology 40 (2006) 4765–4770.
[7] J.M. Stokke, D.W. Mazyck, Environmental Science and Technology 42 (2008) 3808–3813.
[8] M.R. Hoffmann, S.T. Martin, W. Choi, D.W. Bahneman, Chemical Reviews 95 (1995) 69–96.
[9] P.F. Biard, A. Bouzaza, D. Wolbert, Environmental Science and Technology 41 (2007) 2908–2914.
[10] S.O. Obare, T. Ito, M.H. Balfour, G.J. Meyer, Nano Letters 3 (2003) 1151–1153.
[11] X.B. Chen, S.S. Mao, Chemical Reviews 107 (2007) 2891–2959.
[12] R. Comparelli, E. Fanizzaa, M.L. Curri, P.D. Cozzoli, G. Mascoloc, R. Passinoc, A. Agostianoa, Applied Catalysis B 55 (2005) 81–91.
[13] C.A. Páez, D. Poelman, J.P. Pirard, B. Heinrichs, Applied Catalysis B 94 (2010) 263–271.
[14] P.A. Bianco, C. Baiocchi, M.C. Brussino, E. Pramauro, P. Savarino, V. Augugliaro, G. Marcì, L. Palmisano, Environmental Science and Technology 35 (2001) 971–976.
[15] P.D. Cozzoli, E. Fanizza, R. Comparelli, M.L. Curri, A. Agostiano, Journal of Physical Chemistry B 108 (2004) 9623–9630.
[16] D. Gumy, S.A. Giraldo, J. Rengifo, C. Pulgarin, Applied Catalysis B 78 (2008) 19–29.
[17] J.A. Rengifo-Herrera, E. Mielczarski, J. Mielczarski, N.C. Castillo, J. Kiwi, C. Pulgarin, Applied Catalysis B 84 (2008) 448–456.
[18] A. Zielińska-Jurek, E. Kowalska, J.W. Sobczak, W. Lisowski, B. Ohtani, A. Zaleska, Applied Catalysis B 101 (2011) 504–514.
[19] M. Janus, A.W. Morawski, Applied Catalysis B 75 (2007) 118–123.
[20] S.M. Zhang, G.K. Zhang, S.J. Yu, X.G. Chen, X.Y. Zhang, Journal of Physical Chemistry C 113 (2009) 20029–20035.
[21] S.M. Sun, W.Z. Wang, L. Zhang, L. Zhou, W.Z. Yin, M. Shang, Environmental Science and Technology 43 (2009) 2005–2010.
[22] S. Ouyang, H.T. Zhang, D.F. Li, T. Yu, J.H. Ye, Z.G. Zou, Journal of Physical Chemistry B 110 (2006) 11677–11682.
[23] Y. Maruyama, H. Irie, K. Hashimoto, Journal of Physical Chemistry B 110 (2006) 23274–23278.
[24] S. Ouyang, N. Kikugawa, D. Chen, Z.G. Zou, J.H. Ye, Journal of Physical Chemistry C 113 (2009) 1560–1566.
[25] Z. Yi, J.H. Ye, N. Kikugawa, T. Kako, S. Ouyang, H. Stuart-Williams, H. Yang, J. Cao, W.J. Luo, Z.S. Li, Y. Liu, R.L. Withers, Nature Materials 9 (2010) 559–564.
[26] Y. Bi, S. Ouyang, N. Umezawa, J. Cao, J.H. Ye, Journal of the American Chemical Society 133 (2011) 6490–6492.
[27] C. Hu, Y.Q. Lan, J.H. Qu, X.X. Hu, A.M. Wang, Journal of Physical Chemistry B 110 (2006) 4066–4072.
[28] Y.P. Liu, L. Fang, H.D. Lu, Y.W. Li, C.Z. Hua, H.G. Yu, Applied Catalysis B 115–116 (2012) 245–252.
[29] T. Hirakawa, Y. Nosaka, Langmuir 18 (2002) 3247–3254.
[30] C.H. An, S. Peng, Y.G. Sun, Advanced Materials 22 (2010) 2570.
[31] M.D. Segall, P.J.D. Lindan, M.J. Probert, C.J. Pickard, P.J. Hasnip, S.J. Clark, M.C. Payne, Journal of Physics: Condensed Matter 14 (2002) 2717–2744.

[32] J.J. Liu, X.L. Fu, S.F. Chen, Y.F. Zhu, Applied Physics Letters 99 (2011) 1919.
[33] P. Wang, B.B. Huang, X.Y. Qin, X.Y. Zhang, Y. Dai, M.H. Whangbo, Inorganic Chemistry 48 (2009) 10697–10702.
[34] M.S. Zhu, P.L. Chen, M.H. Liu, ACS Nano 5 (2011) 4529–4536.
[35] I.M. Arabatzis, T. Stergiopoulos, M.C. Bernard, D. Labou, S.G. Neophytides, P. Falaras, Applied Catalysis B 42 (2003) 187–201.
[36] M.A. Butler, Journal of Applied Physics 48 (1977) 1914–1920.
[37] H.G. Yu, J.G. Yu, B. Cheng, M.H. Zhou, Journal of Solid State Chemistry 179 (2006) 349–354.
[38] S.B. Zhu, T.G. Xu, H.B. Fu, J.C. Zhao, Y.F. Zhu, Environmental Science and Technology 41 (2007) 6234–6239.
[39] G.L. Huang, S.C. Zhang, T.G. Xu, Y.F. Zhu, Environmental Science and Technology 42 (2008) 8516–8521.
[40] H. Tsutomu, Langmuir 18 (2002) 247–3254.
[41] X. Zhou, C. Hu, X. Hu, T. Peng, J. Qu, Journal of Physical Chemistry C 114 (2010) 2746–2750.
[42] L. Kuai, B.Y. Geng, X.T. Chen, Y.Y. Zhao, Y.C. Luo, Langmuir 26 (2010) 18723–18727.
[43] P. Christopher, H.L. Xin, S. Linic, Nature Chemistry 3 (2011) 467–472.
[44] J.G. Yu, G.P. Dai, B.B. Huang, Journal of Physical Chemistry C 113 (2009) 16394–16401.
[45] J.G. Yu, J.F. Xiong, B. Cheng, S.W. Liu, Applied Catalysis B 60 (2005) 211–221.
[46] C. Chen, W. Ma, J.C. Zhao, Chemical Society Reviews 39 (2010) 4206–4219.
[47] M. Cheng, W. Song, W. Ma, C. Chen, J.C. Zhao, J. Lin, H.Y. Zhu, Applied Catalysis B 77 (2008) 355–363.